


# Comparison of discrete-time sliding mode control algorithms for seismic control of buildings with magnetorheological fluid dampers

Muaz Kemerli<sup>1</sup> , Özge Şahin<sup>2</sup> , İrfan Yazıcı<sup>3</sup>, Naci Çağlar<sup>2,4</sup>, and Tahsin Engin<sup>1</sup>

Journal of Vibration and Control  
2023, Vol. 29(7-8) 1752–1765  
© The Author(s) 2022  
Article reuse guidelines:  
[sagepub.com/journals-permissions](https://sagepub.com/journals-permissions)  
DOI: 10.1177/10775463211070062  
[journals.sagepub.com/home/jvc](https://journals.sagepub.com/home/jvc)  


## Abstract

Semi-active control implementations for structures are gaining considerable attention in civil engineering. This paper presents a method for the design and implementation of the discrete-time sliding mode controller with a hybrid control strategy, based on Gao's reaching law and the variable rate reaching law, for practical applications in civil structures by using magnetorheological (MR) dampers. The structure is modeled as a five-degree-of-freedom lumped mass system, controlled by an MR damper placed in between the ground and the first floor. The MR damper is experimentally tested and its behavior is represented by using modified Bouc–Wen model and artificial neural network (ANN) as forward and inverse models, respectively. The five-story building is simulated under the seismic excitation of El Centro earthquake along with the historical earthquake records, Northridge and Kobe. It is demonstrated that the hybrid control strategy yields better results regarding the energy consumption of the controller and time-averaged structural responses by eliminating the chattering, compared to Gao's controller.

## Keywords

sliding mode control, magnetorheological damper, semi-active control, neural network, Gao controller, hybrid controller, discrete-time

## 1. Introduction

Earthquakes occur all around the world for over a million years, recognized as one of the natural hazards. Earthquakes sometimes cause thousands of deaths and injuries, loss of property, and leave many people homeless. The tragic consequences of earthquakes show that the response of the structures to seismic events is of vital importance. In recent decades, intelligent control of buildings has been attracting considerable interest in civil engineering for the mitigation of seismic responses against earthquake loads (Spencer and Sain, 1997). Seismic energy absorbing systems begin to play an important role in improving the seismic performance of the structures.

Three types of energy-absorbing systems have been used in the structures, namely, active control, passive control, and semi-active control. Active control systems can provide high performance by damping the vibration in a wide frequency range. However, they have a risk of destabilizing the structure by adding energy to the system. The stability problems, large external power requirements, and high-cost maintenance are some of

the main challenges of the active control systems. On the other hand, although passive control does not require an external energy source and is designed depending on the structural response, it does not have the ability to adapt itself to the changing external loads. The semi-active control is a promising alternative, combining the best features of active and passive

<sup>1</sup>Department of Mechanical Engineering, Sakarya University, Sakarya, Turkey

<sup>2</sup>Department of Civil Engineering, Sakarya University, Sakarya, Turkey

<sup>3</sup>Department of Electrical & Electronics Engineering, Sakarya University, Sakarya, Turkey

<sup>4</sup>Department of Civil Engineering, Faculty of Technology Sakarya University of Applied Sciences, Sakarya, Turkey

Received: 27 March 2021; revised: 15 November 2021; accepted: 11 December 2021

### Corresponding author:

Muaz Kemerli, Department of Mechanical Engineering, Sakarya University, Kemalpaşa mah. Üniversite cad, Muhendislik fak, M7 Blok Oda: 7312, Sakarya 54050, Turkey.  
Email: [mkemerli@sakarya.edu.tr](mailto:mkemerli@sakarya.edu.tr)

control at the same time (Housner et al., 1997; Spencer and Sain, 1997; Symans and Constantinou, 1999). A semi-active control system can generally provide the desired performance without requiring a large external energy source which is critical in seismic hazards. The semi-active devices which absorb and store the vibration energy are always stable because it generates the control signal according to the responses of the structure (Luca et al., 2005).

In vibration control applications, one of the most popular devices is the magnetorheological (MR) damper, having attractive features such as quick response to the command signal, low power requirement, low cost, high reliability, and stability. Considering the control of the structures, the MR dampers have proved their superiority over the other semi-active devices such as friction-controlled isolators and variable orifice dampers, owing to their simplicity and practical design (Spencer and Sain, 1997). On the other hand, the main challenge for MR dampers is to design an appropriate control strategy to achieve the desired performance by dealing with the non-linear behavior of the MR damper, especially with the complex hysteretic dynamics (Çeşmeci and Engin, 2010). The controller also must be simple, effective, robust, and suitable for real-time implementation.

Various types of control algorithms have been applied to semi-active control devices in the literature for the mitigation of seismic vibrations (Jansen and Dyke, 2000). The linear quadratic regulator (LQR) and linear quadratic Gaussian (LQG) control algorithms are usually employed as a baseline for the assessment of other control algorithms (Dyke and Spencer, 1997; Xu et al., 2000; Yoshida and Dyke, 2004). Proportional-Integral-Derivative controller (PID) and  $H_\infty$  are some of the other implemented control strategies in the literature (Chen et al., 2010; Choe, 2015). Some researchers have also introduced intelligent control strategies such as Fuzzy Logic (FL) or Artificial Neural Network (ANN) (Bitaraf et al., 2010; Chang and Zhou, 2002; Yan and Zhou, 2006). Sliding mode control (SMC) is also a popular control strategy due to its robustness against the parametric uncertainties, external disturbances, and parameter variations by keeping the system trajectory in the so-called “sliding surface” (Özbay et al., 2017; Utkin, 1993; Young et al., 1999). Furthermore, compared to other non-linear control methods, SMC is relatively easy to be applied to any system (Slotine and Li, 1990). In the last decades, SMC has also been introduced for semi-active structural control to deal with the structural uncertainties and disturbances (Bhaiya et al., 2019; Enríquez-Zárate et al., 2015; Fali et al., 2019; Li and Liang, 2018; Mamat et al., 2020). One of these studies has proposed an adaptive SMC designed to control the MR damper, which is coupled to the clipped optimal algorithm (Fali et al., 2019). The performance of the designed controller

in terms of the  $J_1$ ,  $J_2$ ,  $J_3$ , and  $J_4$  indexes was investigated in a three-story scaled structure excited under two earthquake records, namely, El Centro 1940 and the Boumerdès 2003. In another study, an adaptive non-singular terminal sliding mode controller (NTSMC) has been offered to suppress the vibration of a three-story scaled building excited under El Centro 1940 and Southern Sumatra 2007 seismic data (Mamat et al., 2020). It was shown that the NTSMC yields better performance than FL and conventional SMC regarding to the mitigation of building vibration. In another work (Enríquez-Zárate et al., 2015), multi-positive position feedback controller combined with SMC was designed to attenuate the undesirable vibrations on a structure. Performance of the designed controller was investigated on a three-story scaled building during the earthquake excitations.

The SMC-based controllers were proposed for MR damper-based semi-active systems to attenuate the vibrations on buildings caused by the earthquakes and have been designed in the continuous-time domain, and some of which are summarized above. On the other hand, since the real-time implementation of the designed controller is realized by using a digital processor such as microcontroller, computer, or embedded PC, the proposed controller should be designed in discrete-time domain. As discrete-time systems have a finite sampling period by nature, continuous-time SMC algorithms cannot be applied directly in discrete-time systems. Therefore, the investigation of discrete time-based SMC for semi-active systems with MR dampers is worth considering. In this study, two discrete-time SMC algorithms based on the reaching law method are proposed for the control of the MR damper, placed on the first floor of a five-story building. The first proposed controller is designed using the Gao reaching-law (GAO) and the second one is designed using the hybrid structure based on the Gao + variable rate reaching-law (HYB). The performance of the proposed discrete-time SMC controllers is investigated in a five-story structural system excited under El Centro earthquake along with historical earthquake records of Kobe and Northridge in terms of  $J_1$ ,  $J_2$ ,  $J_3$ ,  $J_4$ ,  $J_5$ , and  $J_6$  criteria. It is shown that the hybrid control strategy yields better results regarding the energy consumption of the controller and the time-averaged structural responses by eliminating the chattering when compared to Gao's controller.

## 2. Structural system modeling

A simple scale structural system is simulated to demonstrate the effectiveness of the proposed control algorithms in reducing the structural responses under earthquake excitations. Five-degree-of-freedom lumped mass system is

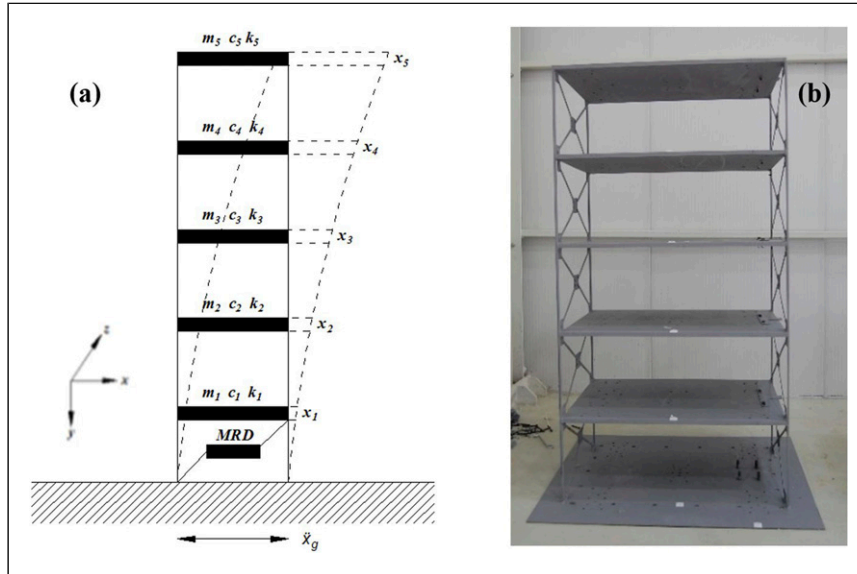


Figure 1. (a) The mathematical model of the structure (b) Experimental structure (MRD: Magnetorheological Damper).

Table 1. Structural parameters.

| Floor masses (kg) | Stiffness (N/m) |
|-------------------|-----------------|
| m1 = 70.57        | k1 = 96000      |
| m2 = 70.57        | k2 = 96000      |
| m3 = 70.57        | k3 = 96000      |
| m4 = 70.57        | k4 = 96000      |
| m5 = 70.57        | k5 = 96000      |

used to represent the model structure in the  $x$ -direction. The first five natural frequencies are 1.67 Hz, 4.88 Hz, 7.69 Hz, 9.87 Hz, and 11.27 Hz, respectively. The mathematical and experimental models are shown in Figure 1. The maximum shear force occurs at the first floor during earthquake excitation. The MR damper is, therefore, attached between the first floor and the ground. The structural model consists of five floors with a 0.60 m x 0.80 m floor area, supported by four columns. The columns have a dimension of 6 x 15 mm, floor slabs are 15 mm thickness steel, and story height is 0.30 m. The mass and stiffness properties are given in Table 1.

Assuming that the semi-active control system tries to keep the structure response in the linear region, the equation of motion can be written as follows

$$[M_s]\ddot{x} + [C_s]\dot{x} + [K_s]x = -M_s\lambda\ddot{x}_g - [\Gamma]f_d \quad (1)$$

where  $\ddot{x}$ ,  $\dot{x}$  and  $x$  are acceleration, velocity, and displacement vector of the structure, respectively.  $M_s$ ,  $C_s$ , and  $K_s$  are mass, damping, and stiffness matrix of the structure with  $5 \times 5$  dimensions.  $\Gamma = [1 \ 0 \ 0 \ 0 \ 0]^T$  is the MR damper's position vector,  $\lambda = [1 \ 1 \ 1 \ 1 \ 1]^T$  is the seismic acceleration effect vector, and  $f_d$  is the acting

control force generated by the MR damper. The proposed structural system mass and stiffness matrices are defined as below:

$$[M_s] = \begin{bmatrix} m_1 & 0 & 0 & 0 & 0 \\ 0 & m_2 & 0 & 0 & 0 \\ 0 & 0 & m_3 & 0 & 0 \\ 0 & 0 & 0 & m_4 & 0 \\ 0 & 0 & 0 & 0 & m_5 \end{bmatrix} \text{ kg}$$

$$[K_s] = \begin{bmatrix} k_1 + k_2 & -k_2 & 0 & 0 & 0 \\ -k_2 & k_2 + k_3 & -k_3 & 0 & 0 \\ 0 & -k_3 & k_3 + k_4 & -k_4 & 0 \\ 0 & 0 & -k_4 & k_4 + k_5 & -k_5 \\ 0 & 0 & 0 & -k_5 & k_5 \end{bmatrix} \frac{N}{m} \quad (2)$$

The damping matrix of a structure according to the Rayleigh damping model is the linear combination of mass and stiffness matrices expressed as follows

$$C_s = \alpha M_s + \beta K_s \quad (3)$$

$$\alpha = \zeta \frac{\omega_1 \omega_2}{\omega_1 + \omega_2} \beta = \zeta \frac{2}{\omega_1 + \omega_2}$$

where  $\zeta$  is the damping ratio of the structural system,  $\alpha$  and  $\beta$  are real scalars.  $\omega_1$  and  $\omega_2$  are circular frequencies. According to this approach, the damping ratio of

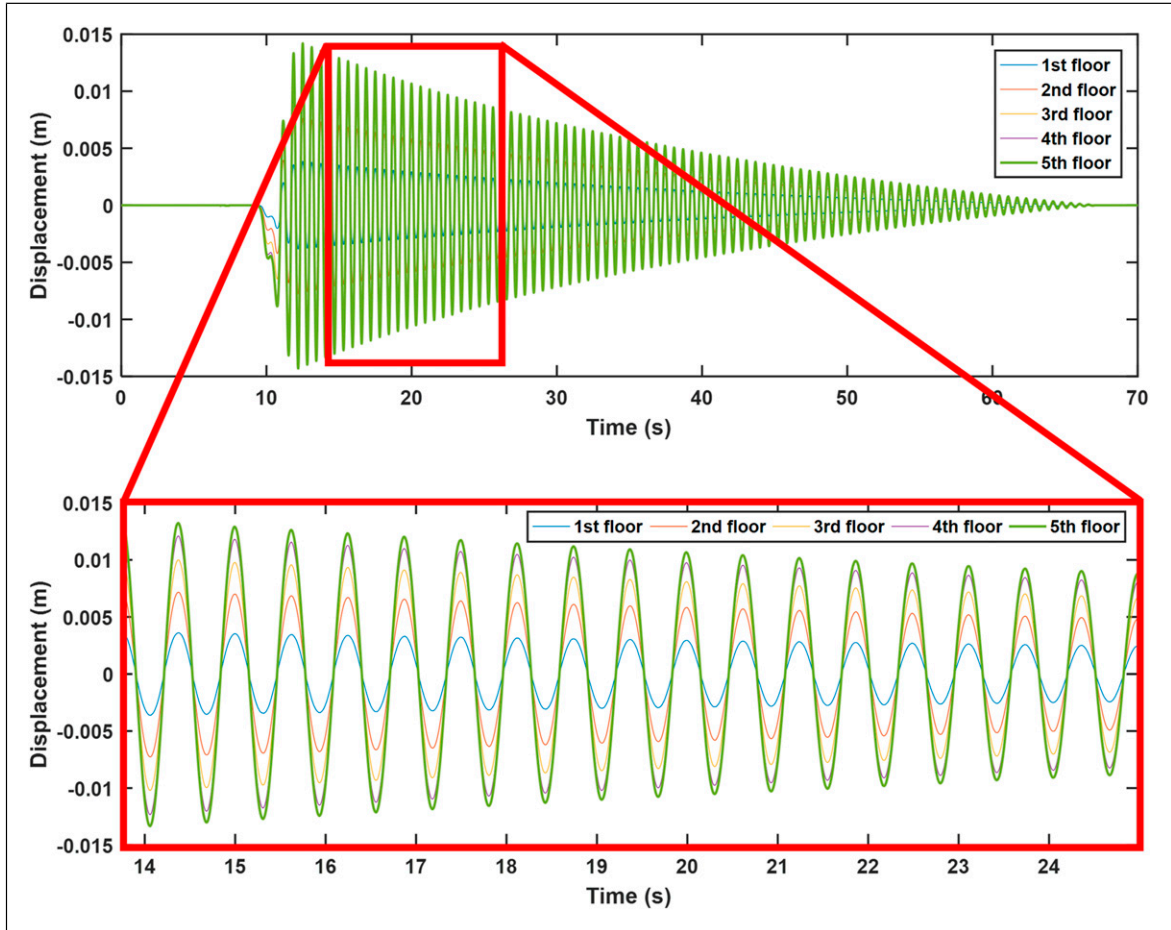


**Figure 2.** Experimental displacement response of free vibration test.

the structural system  $\zeta = 0.0038$  is obtained through the free vibration measurement data represented in Figure 2.

The structural system damping matrix is written below:

$$[C_s] = \begin{bmatrix} 50.72 & -23.59 & 0 & 0 & 0 \\ -23.59 & 50.72 & -23.59 & 0 & 0 \\ 0 & -23.59 & 50.72 & -23.59 & 0 \\ 0 & 0 & -23.59 & 50.72 & -23.59 \\ 0 & 0 & 0 & -23.59 & 27.108 \end{bmatrix} \frac{Ns}{m} \tag{4}$$

Rewriting the equation of motion in the state-space representation of the structural system,

$$\dot{X} = AX + BU$$

$$Y = CX + DU \tag{5}$$

where  $X = [x \dot{x}]^T$  is the state vector of the system. State matrix ( $A$ ), input matrix ( $B$ ), output matrix ( $C$ ), and

feedforward matrix ( $D$ ) are the state-space matrices presented as:

$$A = \begin{bmatrix} 0_{nxn} & I_{nxn} \\ [-M_s^{-1}K_s] & [-M_s^{-1}C_s] \end{bmatrix}$$

$$B = \begin{bmatrix} 0 \\ -[\lambda] \end{bmatrix}$$

$$C = \begin{bmatrix} I_{nxn} & 0_{nxn} \\ 0_{nxn} & I_{nxn} \\ [-M_s^{-1}K_s] & [-M_s^{-1}C_s] \end{bmatrix}$$

$$D = \begin{bmatrix} 0 \\ 0 \\ -[\lambda] \end{bmatrix} \tag{6}$$

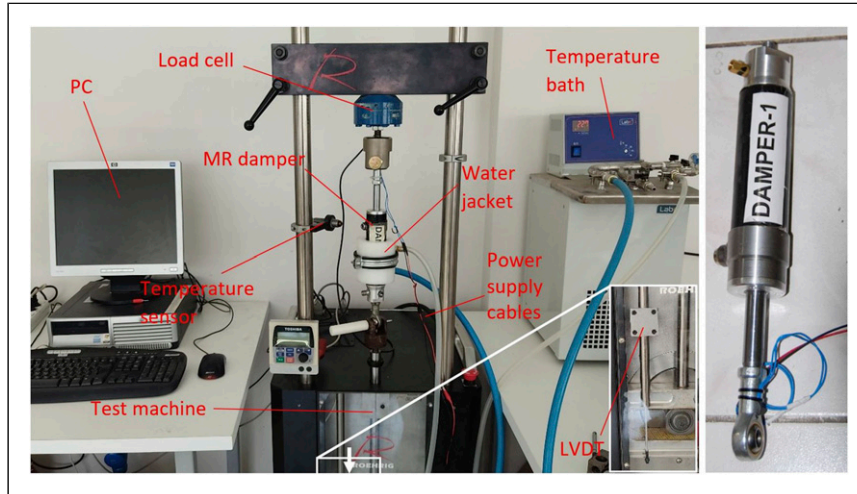


**Figure 3.** (left) The test setup and (right) the produced MR damper.

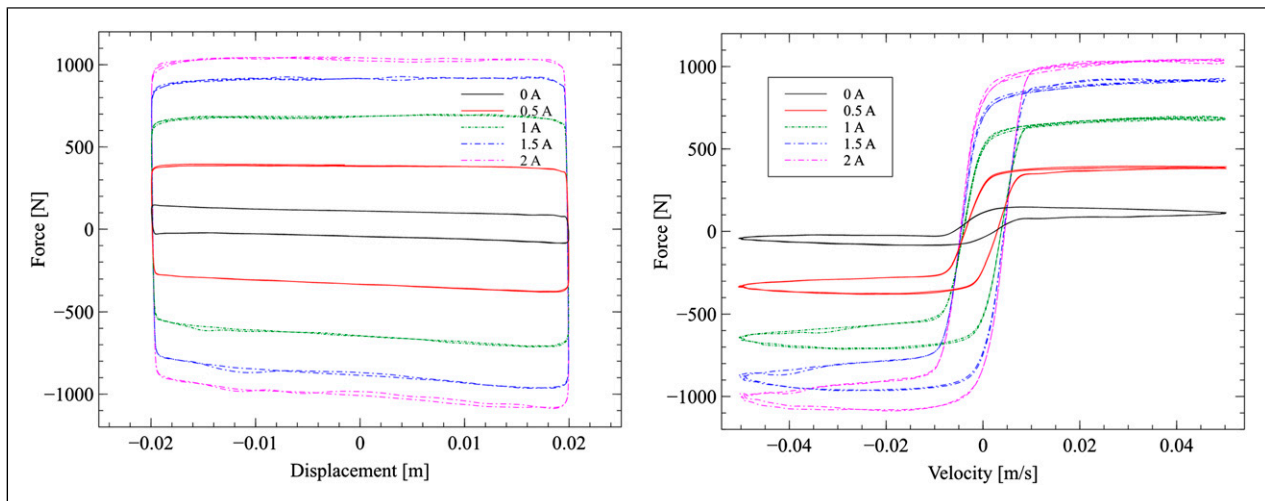


**Figure 4.** (left) Force–displacement and (right) force–velocity response of the MR damper under sinusoidal motion at different currents.

Equations (5) and (6) are then used in the simulation model discussed in Section 5.

### 3. Magnetorheological damper modeling

Magnetorheological dampers are a type of semi-active absorbers containing microscale iron particles suspended in a carrier fluid such as silicone oil called MR fluid. Under the magnetic field, the iron particles become aligned and create a chain-like structure. This structure causes an extra resistance to the flow and keeps the fluid stable if the shear stress is under the yield stress. The yield stress of the fluid can be varied by changing the magnitude of the magnetic field. This provides researchers a wide area to implement these devices in many kinds of control applications.

Modeling of an MR damper is a quite complicated task since the response of an MR damper to the input current,

displacement, and velocity is non-linear and exhibits a hysteretic behavior. Besides, the force response of the MR damper is frequency-dependent (Hemmatian et al., 2018). All these different physical conditions make the modeling of the MR damper challenging. The early parametric models were based on the visco-plastic behavior of the MR fluid and depend on simple assumptions by considering a Bingham plastic fluid (Stanway et al., 1987). Unfortunately, these models were not capable of modeling the non-linear characteristics of an MR damper. In the late 1990s, a new model has been proposed by Spencer et al. (Spencer et al., 1997). This model was an improved version of the classical Bouc–Wen model for MR dampers, namely, the modified Bouc–Wen model, and it is widely accepted among researchers. The most important feature of this model was its ability to model the hysteresis behavior in a precise and simple way apart from the classical Bouc–Wen



and other primitive models. Different models have also been proposed and compared (Sahin et al., 2010), such as the LuGre friction model (Jiménez and Álvarez-Icaza, 2005), the Dahl friction model (Zhou and Qu, 2002), and different algebraic models such as the Kwok model (Kwok et al., 2006). Yet, the modified Bouc–Wen model has remained the most popular among researchers owing to its simplicity and robustness.

Non-parametric modeling of MR dampers has also become an intense research area in the last decade since computers have been improved. Neural Network (NN) and Fuzzy Logic (FL) are the leading non-parametric modeling methods of MR dampers and many studies can be found in the literature (Choi et al., 2004; Wang and Liao, 2005; Xu et al., 2003). The non-parametric models are in a large variety due to their diverse nature.

The controllers of MR dampers are either designed to predict the control signal as current or as force. Estimating the force as the control signal provides more robust control as it matches well with the structure dynamics. Hence, it is adopted in this study. In this case, the force should be converted to current via an inverse model of the MR damper which brings an extra conversion box in the control diagram. To represent this, the forward model of the MR damper is created as a parametric model via the modified Bouc–Wen model, while the inverse MR damper model is created via ANN since the parametric models are generally weak in inverse modeling of the MR damper.

An MR damper was produced for the experimental study (Kemerli and Engin, 2021). Tests were conducted at Sakarya University Applied Fluid Dynamics Laboratory (AFDL). A Roehrig MK-2150 test device was used along with the SHOCK 6.3 software. GWInstek brand, 3223 model, digitally controlled power supply, was used to provide the direct current (DC). The force was measured with a 22 kN load cell and the displacement was measured with a linear variable differential transformer (LVDT). The test setup and the produced MR damper are presented in Figure 3. The MR damper has a maximum stroke of 0.06, corresponding to a ±0.03 m displacement range. Tests were conducted from 0 A to 1 A with an increment of 0.1 A, and from 1 A to 2 A with an increment of 0.5 A, under the sinusoidal linear motion with a velocity range of ±0.05 m/s, and a displacement range of ±0.02 m, which corresponds to a frequency of 0.398 Hz. Since the temperature of the MR damper tends to increase during the continuous operation and affects the response of the MR damper, the temperature was kept constant at the room temperature of 20°C by a temperature bath which is connected to the water jacket covering the MR damper and the temperature was monitored by a temperature sensor.

The force–displacement and force–velocity results of the tests for 0 A, 0.5 A, 1 A, 1.5 A, and 2 A are given in

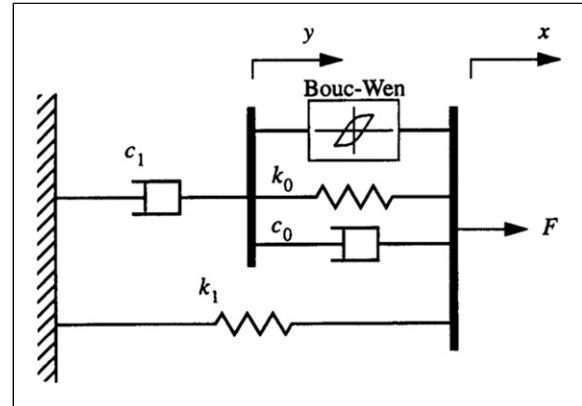


Figure 5. Mechanical model of the modified Bouc–Wen model (Spencer et al., 1997).

Figure 4. The gas force of the MR damper is estimated as 60 N in the positive direction during the compression stroke, and the friction force is estimated as 53 N from the experiments. The friction force may vary depending on the velocity of the MR damper. In the determination of modified Bouc–Wen parameters and the inverse ANN model, the raw data was used, and there is no offset applied in order to simulate the real conditions.

The mechanical model of the modified Bouc–Wen model, shown in Figure 5, can be expressed with equations (7)–(9) (Spencer et al., 1997).

$$f(t) = c_1 \dot{y} + k_1(x - x_0) \tag{7}$$

$$\dot{y} = \frac{1}{c_0 + c_1} \left[ \alpha_{bw} z + c_0 \dot{x} + k_0(x - y) \right] \tag{8}$$

$$\dot{z} = -\gamma \left| \dot{x} - \dot{y} \right| z |z|^{n-1} - \beta_{bw} (\dot{x} - \dot{y}) |z|^n + A (\dot{x} - \dot{y}) \tag{9}$$

The parameters of  $c_0$  and  $\alpha_{bw}$  are modeled as first-degree and  $c_1$  as second-degree polynomials since these parameters are dependent on the input current.  $f$  represents the MR damper force and the coefficients of  $A, \beta_{bw}, \gamma, k_0, k_1, n$ , and  $x_0$  are the constants identified by using the test results. The response time of the MR damper is dependent on the characteristics of the MR damper and the change rate of the input current. This relation is characterized with a first-order filter in equation (10) where  $\eta$  is the response coefficient, and  $u$  and  $v$  represents the actual and previous signal, respectively (Spencer et al., 1997). The response time of the MR damper is measured by using open-loop response and  $\eta$  was calculated as  $100 \text{ s}^{-1}$ .

$$\dot{u} = -\eta(u - v) \tag{10}$$

The velocity range and the frequency used in the simulation are close to those in the MR damper tests. The coefficients of the Bouc–Wen model are presented in Table 2.

**Table 2.** The coefficients of the modified Bouc–Wen model.

| Coefficient  | Value | Coefficient    | Value  |
|--------------|-------|----------------|--------|
| A            | 2900  | $\alpha_{bw}a$ | 6819   |
| $\beta_{bw}$ | 2350  | $\alpha_{bw}b$ | 1461   |
| $\gamma$     | 4000  | $c_0a$         | 746.3  |
| $k_0$        | 2     | $c_0b$         | -165.2 |
| $k_1$        | 0     | $c_1a$         | 73700  |
| $n$          | 4     | $c_1b$         | 131100 |
| $\eta$       | 100   | $c_1c$         | 17140  |
| $x_0$        | 0     |                |        |

\*  $\alpha_{bw}$  and  $c_0$  are calculated as first-degree and  $c_1$  is calculated as a second-degree polynomial regarding the input current.

The NN model of the MR damper is created via “fitnet” function in the MATLAB NN tool. The model contains five hidden layers and one output layer, trained by the Levenberg–Marquardt algorithm with the “trainlm” function.

The schematic view of the controller is shown in Figure 6. According to this scheme, the desired control force, calculated by the controller, is first converted to the input current by using the inverse MR damper model. This corresponds to a 3-input 1-output NN structure as displacement, velocity, and desired force are the inputs and current is the output. The obtained current is then converted to the force response of the MR damper acting on the building by using the Bouc–Wen mathematical model. This time, current, displacement, and velocity are the inputs and acting force is the output.

The output signal is applied to the structure as the acting force which will be discussed further in Section 5.

#### 4. Control algorithm design

In a discrete-time sliding mode design, a control law that forces and holds the closed-loop system trajectory in the sliding surface is needed. In this study, Gao’s reaching law (GAO) and a hybrid control strategy, based on Gao’s reaching law and the variable rate reaching law (HYB), is used. In this section, the general form of the design process of these control laws, which is detailed in (Li and Song, 2007; Weibing et al., 1995; Yao et al., 2000), is given.

At first, since the proposed controllers are designed in discrete-time, the system state-space model given in equation (5) should be transformed into a discrete-time state-space form with a sampling time  $T_s$  resulting in

$$x(k+1) = \Phi x(k) + \Gamma u(k) \quad (11)$$

The generic switching function can be defined as (Weibing et al., 1995)

$$s(k) = Sx(k) = S_1x_1(k) + x_2(k) \quad (12)$$

where  $S = [S_1 \ 1]$  is a constant vector.

Starting with the Gao’s reaching condition (Weibing et al., 1995), it can be defined as

$$s(k+1) = (1 - qT_s)s(k) - \varepsilon T_s \text{sgn}(s(k)) \quad (13)$$

where  $\varepsilon > 0, q > 0, (1 - qT_s) > 0, T_s$  is the sampling period.

From equations (11) and (12), it can be written as

$$s(k+1) = S\{\Phi x(k) + \Gamma u(k)\} \quad (14)$$

Comparing this equation with reaching law in equation (13), one can get the following equation:

$$S\Phi x(k) + S\Gamma u(k) = (1 - qT_s)s(k) - \varepsilon T_s \text{sgn}(s(k)) \quad (15)$$

Solving equation (15) for  $u(k)$ , the control law based on Gao’s reaching law (GAO) can be found as

$$u_g(k) = -(S\Gamma)^{-1}[S\Phi x(k) - (1 - qT_s)s(k) + \varepsilon T_s \text{sgn}(Sx(k))] \quad (16)$$

The variable rate reaching law can be defined as follows (Yao et al., 2000)

$$s(k+1) = s(k) - \varepsilon T_s \|x(k)\|_1 \text{sgn}(s(k)) \quad (17)$$

where  $\|x(k)\|_1 = \sum_{i=1}^n |x_i(k)|$  is the norm of the vector  $x$ .

From equation (17), if  $s(k) = 0^+$ , then

$$s(k+1) = -\varepsilon T_s \|x(k)\|_1 \quad (18)$$

and if  $s(k) = 0^-$ , then

$$s(k+1) = \varepsilon T_s \|x(k)\|_1 \quad (19)$$

From equations (14) and (17), the control law based on the variable rate reaching law is obtained as

$$u_{vr}(k) = -(S\Gamma)^{-1}[S\Phi x(k) - Sx(k) + \varepsilon T_s \|x(k)\|_1 \text{sgn}(Sx(k))] \quad (20)$$

Finally, by using  $u_g(k)$  and  $u_{vr}(k)$ , the hybrid control law (HYB) is obtained as below:

$$u_{hyb}(k) = \begin{cases} u_g(k), & \text{if } \|x(k)\|_1 > 1 \\ u_{vr}(k), & \text{if } \|x(k)\|_1 \leq 1 \end{cases} \quad (21)$$

Although there are various approaches in determining the  $S$ ,  $\varepsilon$ , and  $q$  coefficients defined for control signals given in equations (15) and (19), the trial-and-error approach is also widely preferred in the literature. Therefore, in the simulation studies, the best fit values of  $S$ ,  $\varepsilon$ , and  $q$  coefficients are obtained by a few trial-and-error steps considering the general conditions given in equation (13) and the  $J_1 - J_6$  criteria which will be discussed in the next section.

## 5. Numerical example

The seismic response of a five-story building structure has been modeled to compare the responses obtained by the proposed control algorithms. The structural system is simulated under El Centro 1940 as a reference earthquake input owing to its ability to represent a wide range of frequency content. As a comparison, Northridge 1994 and Kobe 1995 earthquakes are also considered briefly to reveal the controller performance under different frequencies. In order to keep the structural response in the elastic region, the earthquake records are scaled with a magnitude of 1, 0.75 and 0.5 for the El Centro, Northridge, and Kobe, respectively. The NS component time-history records of the earthquakes are presented in Figure 7.

Figure 8 shows the architecture of the semi-active controller of the MR damper. The control algorithm uses the displacement and velocity states of the structure to generate the control signal as the desired reference force. This signal is then converted to the input current by the inverse ANN model, and the response of the MR damper to the input current is calculated by the forward modified Bouc–Wen MR damper model. Finally, the

acting control force is applied to the first floor through an MR damper with the earthquake signal applied to the structure.

The uncontrolled and semi-actively controlled structural responses of the first and fifth story under El Centro earthquake are depicted in Figure 9 and Figure 10, respectively. Maximum interstory drift under the El Centro earthquake for all floors is shown in Figure 11.

Both controllers show a similar displacement response on the first floor and HYB generates a slightly better acceleration response, shown in Figure 9. As for the fifth floor shown in Figure 10, the success of the HYB controller is evident for both displacement and acceleration responses, which indicates the increasing performance of the HYB controller with the number of floors. The maximum interstory drift, plotted in Figure 11, is similar for both controllers. Since the MR damper is placed on the first floor, the reduction in the maximum interstory drift of the first floor is larger than others, as expected.

In order to demonstrate the effectiveness of controllers in reducing vibrations under earthquake excitations, the

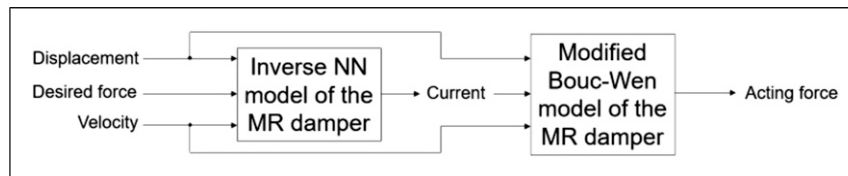


Figure 6. Schematic view of the MR damper simulation model.

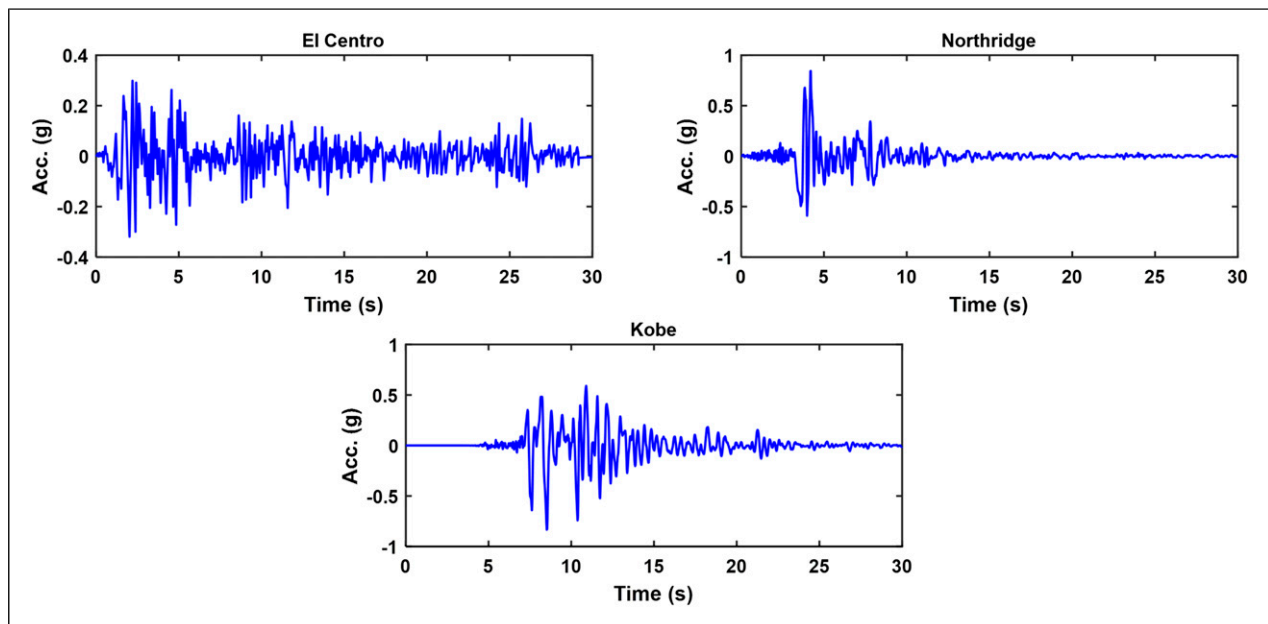


Figure 7. Time-history records of the historical earthquakes used in simulations.



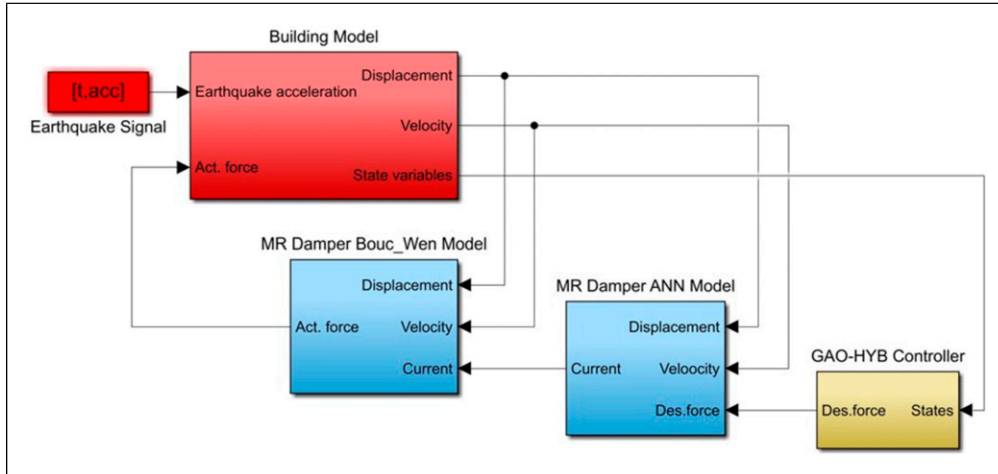


Figure 8. General block diagram of the semi-active control design.

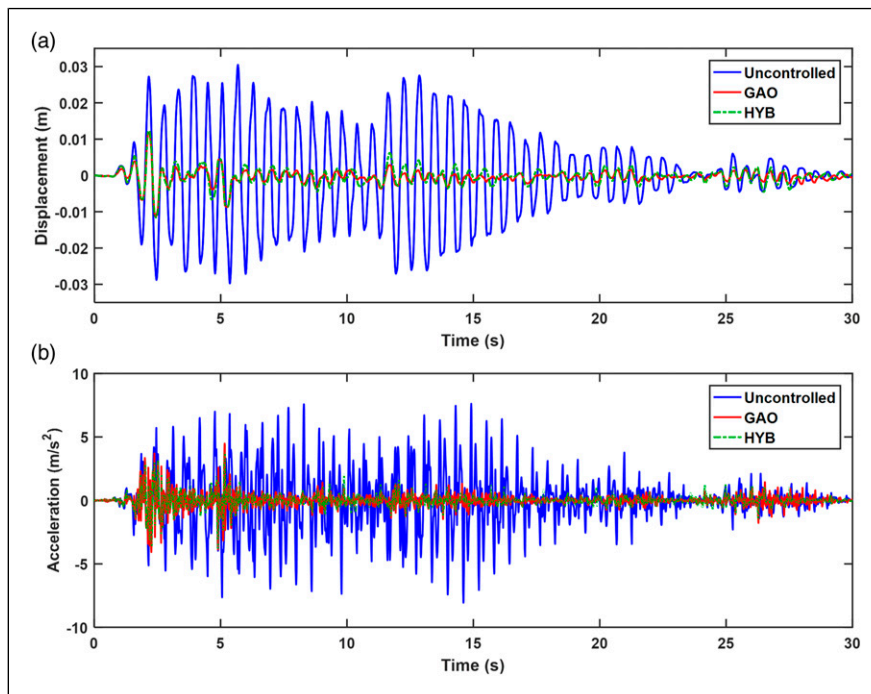


Figure 9. (a) Displacement and (b) acceleration response of the first floor under El Centro earthquake.

results are also evaluated by the performance indexes used in the literature for the semi-active controlled and uncontrolled case of the MR damper (Ohtori et al., 2004). In Table 3, the summary of the selected evaluation criteria for the structural system is presented where  $d_i(t)$  is the interstorey drift over the time history of the earthquake,  $h_i$  is the height of the stories,  $\delta^{max}$  is the maximum interstorey drift ratio of the uncontrolled case, and  $\ddot{x}_{ai}(t)$  and  $\ddot{x}_a^{max}$  are the absolute acceleration of the controlled and uncontrolled structure, respectively.  $m_i$  is the mass of the corresponding floor and  $F_b^{max}$  is the maximum base shear of the uncontrolled structure.  $J_4 - J_6$  are defined as the

normed-based forms of the considered variables in  $J_1 - J_3$  where the norm,  $\|\cdot\|$ , is calculated, using the following equation

$$\|\cdot\| \equiv \sqrt{\frac{1}{t_f} \int_0^{t_f} [\cdot]^2 dt} \quad (22)$$

$t_f$  is the simulation time, which is larger enough to reduce the seismic vibration to a neglectable level (Ohtori et al., 2004).

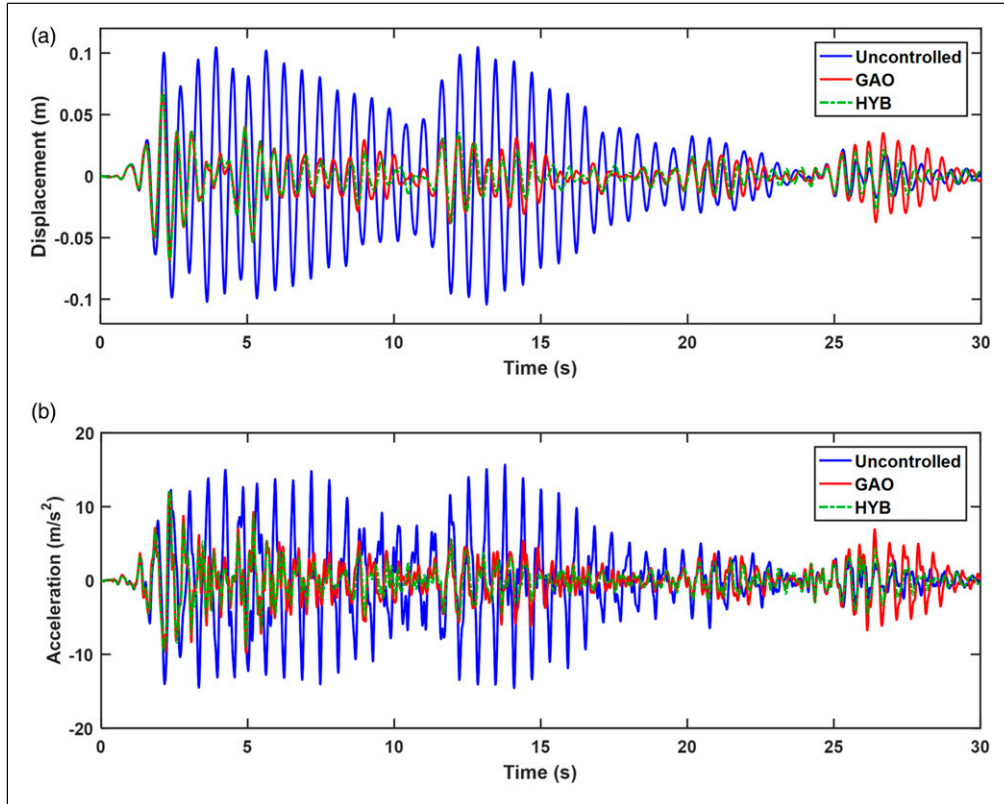


Figure 10. (a) Displacement and (b) acceleration response of the fifth floor under El Centro earthquake.

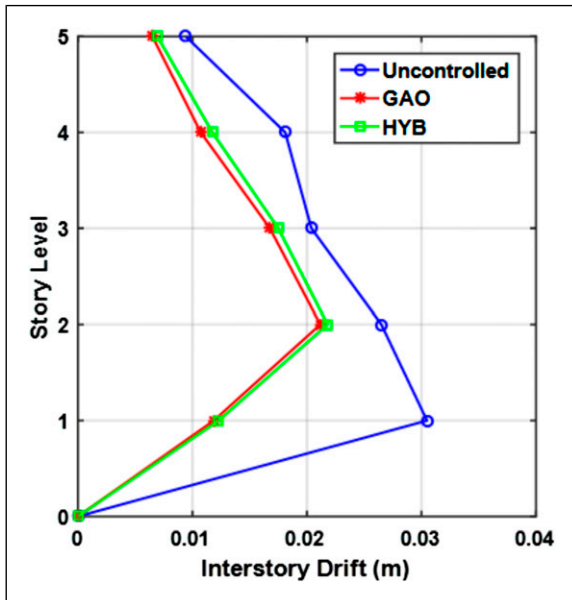


Figure 11. Maximum interstory drift under El Centro earthquake.

Table 3. Summary of the selected evaluation criteria.

| Peak interstory drift ratio   | Normed interstory drift ratio  |
|---|--|
| $J_1 = \max \left[ \frac{\max_{t,j} \left  \frac{d_j(t)}{h_j} \right }{\delta^{max}} \right]$ | $J_4 = \max \left[ \frac{\max_i \frac{d_i(t)}{h_i}}{\delta^{max}} \right]$   |
| Level acceleration  | Normed level acceleration  |
| $J_2 = \max \left[ \frac{\max_i \left  \ddot{x}_{ai}(t) \right }{\ddot{x}_a^{max}} \right]$   | $J_5 = \max \left[ \frac{\max_i \ddot{x}_{ai}(t)}{\ddot{x}_a^{max}} \right]$ |
| Base shear  | Normed base shear  |
| $J_3 = \left[ \frac{\max \left  \sum_i m_i \ddot{x}_{ai}(t) \right }{F_b^{max}} \right]$      | $J_6 = \left[ \frac{\max \sum_i m_i \ddot{x}_{ai}(t)}{F_b^{max}} \right]$    |

The results of the controllers based on the evaluation criteria are shown in Table 4 for historical earthquakes. The magnitude of the displacement response of structures during the seismic control with MR dampers is related to structural safety. Therefore, in the design of the controllers, first-floor displacement and velocity responses are selected as input variables for both controllers.

**Table 4.** Evaluation criteria indices of the proposed control algorithms.

| Criteria | El Centro |       |      | Kobe    |       |       | Northridge |       |       |
|----------|-----------|-------|------|---------|-------|-------|------------|-------|-------|
|          | Uncont.   | GAO   | HYB  | Uncont. | GAO   | HYB   | Uncont.    | GAO   | HYB   |
| $J_1$    | 1.00      | 0.39  | 0.40 | 1.00    | 0.54  | 0.52  | 1.00       | 0.59  | 0.62  |
| $J_2$    | 1.00      | 0.98  | 1.03 | 1.00    | 1.04  | 1.00  | 1.00       | 1.08  | 1.05  |
| $J_3$    | 1.00      | 0.82  | 0.83 | 1.00    | 0.84  | 0.81  | 1.00       | 0.93  | 0.94  |
| $J_4$    | 1.00      | 0.23  | 0.20 | 1.00    | 0.52  | 0.53  | 1.00       | 0.40  | 0.39  |
| $J_5$    | 1.00      | 0.52  | 0.44 | 1.00    | 1.07  | 1.01  | 1.00       | 0.79  | 0.77  |
| $J_6$    | 1.00      | 0.47  | 0.40 | 1.00    | 1.00  | 0.94  | 1.00       | 0.73  | 0.71  |
| $E_u$    | 1.00      | 17.40 | 9.60 | 1.00    | 18.00 | 14.02 | 1.00       | 18.43 | 15.97 |

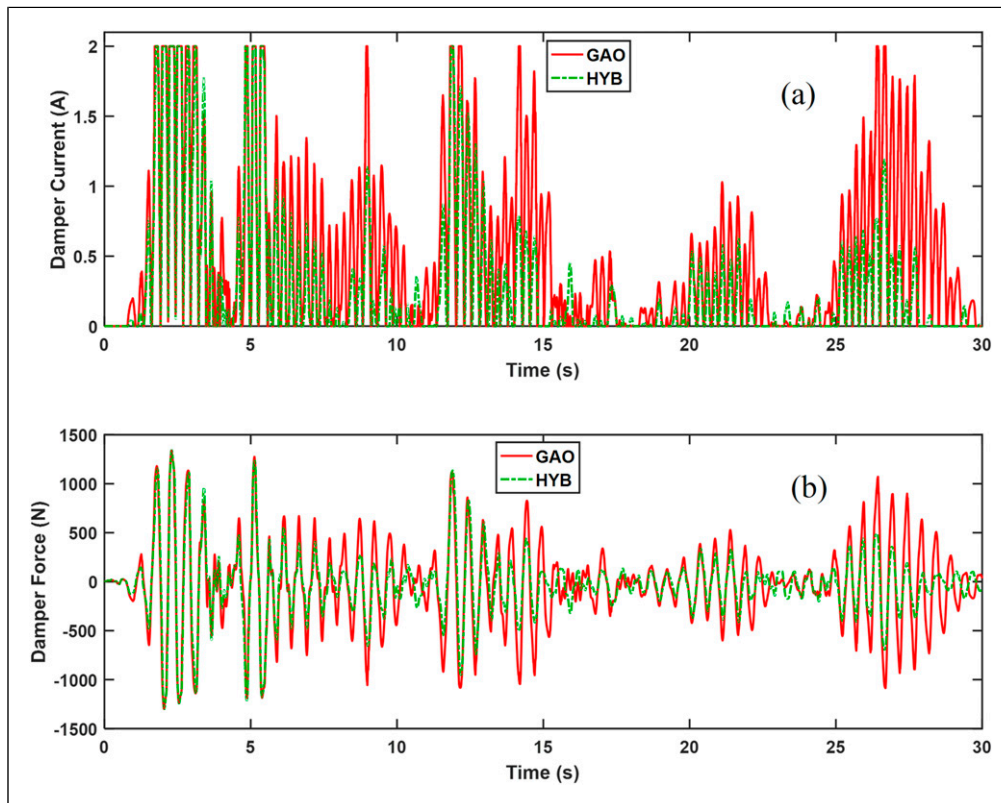


**Figure 12.** Calculated (a) MR damper current and (b) acting force under the El Centro earthquake.

The energy of the control signal is used to evaluate the effectiveness of the controllers as shown below where  $u$  is the input

$$E_u = \int_0^{t_f} u^2 dt \tag{23}$$

The simulation results show that the GAO and HYB controllers can decrease the maximum displacement response to a similar level by reducing the peak interstory drift ratio ( $J_7$ ) up to 60%. On the other hand, the acceleration

response reduction in vibration control of structures is related to the comfort level of the occupants. Although both algorithms are not effective in reducing the peak response of acceleration levels ( $J_2$ ), they are quite successful in the normed ones ( $J_5$ ) except Kobe. The energy transferred to the structure is described as the base shear force ( $J_3$ ). The proposed controllers reduced the base shear force at a close level compared to each other. Slight enhancements in some cases in the  $J_2$  and  $J_3$  indexes of GAO might be a result of the chattering, sharp signal variation generated by GAO reaching law. In contrast, HYB controller compromises with the performance of the maximum indexes since it uses a variable

reaching law to avoid chattering. The GAO and HYB control algorithms are more effective on normed performance indexes ( $J_4 - J_6$ ). Considering the El Centro earthquake, the decreases in normed interstory drift ratio ( $J_4$ ) are 77% and 80%, and the decreases in normed level accelerations ( $J_5$ ) are 48% and 56%. Normed base shear ( $J_6$ ) is also decreased by 53% and 60% for the GAO and HYB controllers, respectively. The results clearly show that the HYB controller is better than GAO regarding the  $J_4 - J_6$  criteria, while the performance is alike for both controllers in terms of  $J_1 - J_3$ .

Another important aspect for the controllers is the energy consumed during the control of the MR damper. The comparison of the acting force and MR damper current signal obtained from the GAO and HYB controllers under El Centro earthquake is shown in Figure 12. As can be seen from Table 4, the energy level of HYB algorithm is almost half of that of GAO. It can also be inferred that HYB controller presents better performance than GAO and consumes less energy. Therefore, HYB controller can work with a limited energy source, which is of high importance in case of an emergency.

Operating at high energy levels also increases the MR damper temperature in real-time applications, causing a performance loss for MR dampers. Besides, varying temperature deteriorates the dynamic structure of the MR damper, eventually causing the controller to create false current signals corresponding to the desired force.

Another issue is that the MR damper becomes less effective in the case of a chattering input signal since it needs a response time in order to change its behavior as mentioned in equation (10). GAO controller generates a rapidly changing and chattering signal to keep the controller on the sliding surface. This might be the cause of the poor performance observed in  $J_4 - J_6$  indexes although it shows a better performance in reducing the maximum acceleration ( $J_2$ ) and base shear force ( $J_3$ ). It must be noted that this performance loss can be larger in real-time applications since the response time is modeled with a simple assumption in the simulation.

## 6. Conclusion

In this study, two different discrete-time sliding mode controllers, namely, HYB and GAO, are investigated under the seismic excitations by using an experimentally validated MR damper model on a five-story building model. The simulation is conducted in discrete-time to understand the response of the controllers in real-time. Numerical simulation results are discussed to evaluate the performance of the semi-active controlled system. The outcomes of the study would be valuable for practical implementations as shown below:

- Considering the structural safety, both controllers show an effective performance in the maximum interstory drift

ratio, shown as  $J_1$  index, with an average value of 0.50 and up to 0.40.

- HYB controller shows significantly better performance in  $J_4 - J_6$  indexes while GAO is slightly better in reducing the maximum values presented in  $J_1 - J_3$  indexes.
- For some cases, the chattering behavior observed in GAO controller results in a slight enhancement in the maximum value indexes  $J_2$  and  $J_3$ , while HYB controller compromises with the maximum value indexes since it uses variable reaching law to avoid chattering.
- The response time of the MR fluid is dependent on the change of the input current. Thus, a chattering input signal results in a longer response time which affects the performance of the controller, as can be seen in the  $J_4 - J_6$  indexes. This effect might be even worse in real-time applications since it is modeled with a first-order filter in the simulation.
- Higher input currents elevate the MR fluid temperature, and it can decrease the performance of the MR damper, and eventually, the controller becomes less effective. Yet, the lower input currents observed in the HYB controller can keep the temperature at reasonable levels.
- Considering the limited energy sources in case of an emergency, HYB controller provides effective damping with lower energy, while GAO controller consumes considerably higher energy, and it is also ineffective in time-averaged indexes,  $J_4$ ,  $J_5$ , and  $J_6$ .
- The reduction rate in the evaluation criteria remains close to each other for both controllers although having different values depending on the applied earthquake signal.

## Declaration of conflicting interests

The authors declare no conflict of interest in preparing this article

## Funding

The author(s) disclosed receipt of the following financial support for the research, authorship, and/or publication of this article: The authors gratefully acknowledge the Scientific and Technological Research Council of Turkey (TUBITAK) for its support of this work under Grant No: 115M363

## ORCID iDs

Muaz Kemerli  <https://orcid.org/0000-0001-5643-8835>

Özge Şahin  <https://orcid.org/0000-0003-0803-7484>

## References

- Bhaiya V, Shrimali MK, Bharti SD, et al. (2019) Modified semi-active control with MR dampers for partially observed systems. *Engineering Structures* 191: 129–147. DOI: [10.1016/j.engstruct.2019.04.063](https://doi.org/10.1016/j.engstruct.2019.04.063).
- Bitaraf M, Ozbulut OE, Hurlebaus S, et al. (2010) Application of semi-active control strategies for seismic protection of



- buildings with MR dampers. *Engineering Structures* 32(10): 3040–3047. Elsevier Ltd. DOI: [10.1016/j.engstruct.2010.05.023](https://doi.org/10.1016/j.engstruct.2010.05.023).
- Çeşmeci Ş and Engin T (2010) Modeling and testing of a field-controllable magnetorheological fluid damper. *International Journal of Mechanical Sciences* 52(8): 1036–1046. DOI: [10.1016/j.ijmecsci.2010.04.007](https://doi.org/10.1016/j.ijmecsci.2010.04.007).
- Chang C-C and Zhou L (2002) Neural network emulation of inverse dynamics for a magnetorheological damper. *Journal of Structural Engineering* 128(2): 231–239. DOI: [10.1061/\(ASCE\)0733-9445\(2002\)128:2\(231\)](https://doi.org/10.1061/(ASCE)0733-9445(2002)128:2(231)).
- Chen Y, Zhang W and Gao H (2010) Finite frequency control for building under earthquake excitation. *Mechatronics* 20(1): 128–142. DOI: [10.1016/j.mechatronics.2009.11.001](https://doi.org/10.1016/j.mechatronics.2009.11.001).
- Choe W-W (2015) Intelligent PID controller and its application to structural vibration mitigation with MR Damper. *Transactions of the Korean Institute of Electrical Engineers* 64(8): 1224–1230. DOI: [10.5370/KIEE.2015.64.8.1224](https://doi.org/10.5370/KIEE.2015.64.8.1224).
- Choi K-M, Cho S-W, Jung H-J, et al. (2004) Semi-active fuzzy control for seismic response reduction using magnetorheological dampers. *Earthquake Engineering & Structural Dynamics* 33(6): 723–736. DOI: [10.1002/eqe.372](https://doi.org/10.1002/eqe.372).
- Dyke SJ and Spencer BF (1997) A comparison of semi-active control strategies for the MR damper. *Proceedings Intelligent Information Systems. IIS'97 1997*: 580–584. DOI: [10.1109/IIS.1997.645424](https://doi.org/10.1109/IIS.1997.645424).
- Enriquez-Zárate J, Silva-Navarro G and Cabrera-Amado A (2015) Semiactive Vibration Control in a Three-Story Building-Like Structure Using a Magnetorheological Damper. *Conference Proceedings of the Society for Experimental Mechanics Series* 2: 475–483. DOI: [10.1007/978-3-319-15248-6\\_48](https://doi.org/10.1007/978-3-319-15248-6_48).
- Fali L, Djermane M, Zizouni K, et al. (2019) Adaptive sliding mode vibrations control for civil engineering earthquake excited structures. *International Journal of Dynamics and Control* 7(3): 955–965. DOI: [10.1007/s40435-019-00559-0](https://doi.org/10.1007/s40435-019-00559-0).
- Hemmatian M, Sedaghati R and Rakheja S (2018) Linear and nonlinear viscoelastic behavior of MR fluids: effect of temperature. In: Volume 1: Development and Characterization of Multifunctional Materials; Modeling, Simulation, and Control of Adaptive Systems; Integrated System Design and Implementation, San Antonio, TX, USA, 10 September 2018. American Society of Mechanical Engineers (ASME). DOI: [10.1115/SMASIS2018-8033](https://doi.org/10.1115/SMASIS2018-8033).
- Housner GW, Bergman LA, Caughey TK, et al. (1997) Structural control: past, present, and future. *Journal of Engineering Mechanics* 123(9): 897–971. DOI: [10.1061/\(ASCE\)0733-9399\(1997\)123:9\(897\)](https://doi.org/10.1061/(ASCE)0733-9399(1997)123:9(897)).
- Jansen LM and Dyke SJ (2000) Semiactive control strategies for MR dampers: comparative study. *Journal of Engineering Mechanics* 126(8): 795–803. DOI: [10.1061/\(ASCE\)0733-9399\(2000\)126:8\(795\)](https://doi.org/10.1061/(ASCE)0733-9399(2000)126:8(795)).
- Jiménez R and Álvarez-Icaza L (2005) LuGre friction model for a magnetorheological damper. *Structural Control and Health Monitoring* 12(1): 91–116. DOI: [10.1002/stc.58](https://doi.org/10.1002/stc.58).
- Kemerli M and Engin T (2021) Numerical analysis of a monotube mixed mode magnetorheological damper by using a new rheological approach in CFD. *Rheologica Acta* 60(1): 77–95. DOI: [10.1007/s00397-020-01252-2](https://doi.org/10.1007/s00397-020-01252-2).
- Kwok NM, Ha QP, Nguyen TH, et al. (2006) A novel hysteretic model for magnetorheological fluid dampers and parameter identification using particle swarm optimization. *Sensors and Actuators A: Physical* 132(2): 441–451. DOI: [10.1016/j.sna.2006.03.015](https://doi.org/10.1016/j.sna.2006.03.015).
- Li H and Song L (2007) Discrete variable structure control design and its application to a power system. In: 2007 2nd IEEE Conference on Industrial Electronics and Applications, Harbin, China, May 2007. IEEE, 990–993. DOI: [10.1109/ICIEA.2007.4318556](https://doi.org/10.1109/ICIEA.2007.4318556).
- Li L and Liang H (2018) Semiactive control of structural nonlinear vibration considering the MR damper model. *Journal of Aerospace Engineering* 31(6): 1–9. DOI: [10.1061/\(ASCE\)AS.1943-5525.0000902](https://doi.org/10.1061/(ASCE)AS.1943-5525.0000902).
- Luca S-G, Chira F and Rosca V-O (2005) Passive active and semi-active control systems in civil engineering. *Buletinul Institutului Politehnic Din Iasi*.
- Mamat N, Yakub F, Shaikh Salim SAZ, et al. (2020) Seismic vibration suppression of a building with an adaptive non-singular terminal sliding mode control. *Journal of Vibration and Control* 26(23–24): 2136–2147. DOI: [10.1177/1077546320915324](https://doi.org/10.1177/1077546320915324).
- Ohtori Y, Christenson RE, Spencer BF, et al. (2004) Benchmark control problems for seismically excited nonlinear buildings. *Journal of Engineering Mechanics* 130(April): 366–385. DOI: [10.1061/\(ASCE\)0733-9399\(2004\)130:4\(366\)](https://doi.org/10.1061/(ASCE)0733-9399(2004)130:4(366)).
- Özbay H, Öncü S and Kesler M (2017) SMC-DPC based active and reactive power control of grid-tied three phase inverter for PV systems. *International Journal of Hydrogen Energy* 42(28): 17713–17722. DOI: [10.1016/j.ijhydene.2017.04.020](https://doi.org/10.1016/j.ijhydene.2017.04.020).
- Şahin I, Engin T and Çeşmeci Ş (2010) Comparison of some existing parametric models for magnetorheological fluid dampers. *Smart Materials and Structures* 19(3): 035012. DOI: [10.1088/0964-1726/19/3/035012](https://doi.org/10.1088/0964-1726/19/3/035012).
- Slotine J and Li W (1990) *Applied Nonlinear Control*.
- Spencer BF and Sain MK (1997) Controlling buildings: a new frontier in feedback. *IEEE Control Systems* 17(6): 19–35. DOI: [10.1109/37.642972](https://doi.org/10.1109/37.642972).
- Spencer BFJ, Dyke SJ, Sain MK, et al. (1997) Phenomenological model for magnetorheological dampers. *Journal of Engineering Mechanics* 123(3): 230–238. DOI: [10.1061/\(ASCE\)0733-9399\(1997\)123:3\(230\)](https://doi.org/10.1061/(ASCE)0733-9399(1997)123:3(230)).
- Stanway R, Sproston JL and Stevens NG (1987) Non-linear modelling of an electro-rheological vibration damper. *Journal of Electrostatics* 20(2): 167–184. DOI: [10.1016/0304-3886\(87\)90056-8](https://doi.org/10.1016/0304-3886(87)90056-8).
- Symans MD and Constantinou MC (1999) Semi-active control systems for seismic protection of structures: a state-of-the-art review. *Engineering Structures* 21(6): 469–487. DOI: [10.1016/S0141-0296\(97\)00225-3](https://doi.org/10.1016/S0141-0296(97)00225-3).
- Utkin VI (1993) Sliding mode control design principles and applications to electric drives. *IEEE Transactions on Industrial Electronics* 40(1): 23–36. DOI: [10.1109/41.184818](https://doi.org/10.1109/41.184818).
- Wang DH and Liao WH (2005) Modeling and control of magnetorheological fluid dampers using neural networks. *Smart Materials and Structures* 14(1): 111–126. DOI: [10.1088/0964-1726/14/1/011](https://doi.org/10.1088/0964-1726/14/1/011).
- Weibing G, Yufu W and Homaifa A (1995) Discrete-time variable structure control systems. *IEEE Transactions on Industrial Electronics* 42(2): 117–122. DOI: [10.1109/41.370376](https://doi.org/10.1109/41.370376).
- Xu YL, Qu WL and Ko JM (2000) Seismic response control of frame structures using magnetorheological/electrorheological dampers. *Earthquake Engineering and Structural Dynamics*



- 29(5): 557–575. DOI: [10.1002/\(SICI\)1096-9845\(200005\)29:5<557::AID-EQE922>3.0.CO;2-X](https://doi.org/10.1002/(SICI)1096-9845(200005)29:5<557::AID-EQE922>3.0.CO;2-X).
- Xu Z-D, Shen Y-P and Guo Y-Q (2003) Semi-active control of structures incorporated with magnetorheological dampers using neural networks. *Smart Materials and Structures* 12(1): 80–87. DOI: [10.1088/0964-1726/12/1/309](https://doi.org/10.1088/0964-1726/12/1/309).
- Yan G and Zhou LL (2006) Integrated fuzzy logic and genetic algorithms for multi-objective control of structures using MR dampers. *Journal of Sound and Vibration* 296(1–2): 368–382. DOI: [10.1016/j.jsv.2006.03.011](https://doi.org/10.1016/j.jsv.2006.03.011).
- Yao Q, Song L and Wen H (2000) Proportional-constant-variable rate control for discrete-time variable structure systems. *Control and Decision* 15(3): 329–332.
- Yoshida O and Dyke SJ (2004) Seismic control of a nonlinear benchmark building using smart dampers.pdf. *Journal of Engineering Mechanics* 130(4): 386–392. DOI: [10.1061/ASCE0733-93992004130:4386](https://doi.org/10.1061/ASCE0733-93992004130:4386).
- Young KD, Utkin VI and Ozguner U (1999) A control engineer's guide to sliding mode control. *IEEE Transactions on Control Systems Technology* 7(3): 328–342. DOI: [10.1109/87.761053](https://doi.org/10.1109/87.761053).
- Zhou Q and Qu W (2002) Two mechanical models for magnetorheological damper and corresponding test verification. *Journal of Earthquake Engineering and Engineering Vibration* 22(4): 144–150.